

# Computer assisted detection and quantification of single adsorbing nanoparticles by differential surface plasmon microscopy

Irina Sidorenko<sup>1</sup> · Shavkat Nizamov<sup>2</sup> · Roland Hergenröder<sup>3</sup> · Alexander Zybin<sup>3</sup> · Alexei Kuzmichev<sup>3</sup> · Bettina Kiwull<sup>4</sup> · Reinhard Niessner<sup>4</sup> · Vladimir M. Mirsky<sup>2</sup>

Received: 23 June 2015 / Accepted: 4 August 2015 / Published online: 15 August 2015  
© Springer-Verlag Wien 2015

**Abstract** Sensitive detection of engineered nanoparticles (NPs) in air and in liquid samples is an important task and still a major challenge in analytical chemistry. Recent work demonstrated that it can be performed using surface plasmon microscopy (SPM) where binding of single NPs to a surface leads to the formation of characteristic patterns in differential SPM images. However, these patterns have to be discriminated from a noisy background. Computer-assisted recognition of nanoparticles offers a solution but requires the development of respective tools for data analysis. Hereby a numerical method for automated detection and characterization of images of single adsorbing NPs in SPM image sequences is presented. The detection accuracy of the method was validated using computer generated images and manual counting. The method was applied for detecting and imaging of gold and silver NPs adsorbing from aqueous dispersions and for soot and NaCl NPs adsorbing from aerosols. The determined adsorption rate was in range 0.1–40 NPs per (s mm<sup>2</sup>) and linearly dependent on the concentration of nanoparticles. Depending on the type of NPs and signal to noise ratio, a probability of recognition of 90–95 % can be achieved.

**Keywords** Nanoparticles · Aerosols · Soot nanoparticles · Surface plasmon resonance (SPR) · Surface plasmon microscopy (SPM) · Image processing · Single nanoparticle detection

## Introduction

The thriving production and application of nanomaterials results in an increasing release of new types of these potentially hazardous materials into the environment. Active absorption of some classes of nanoparticles by biological cells makes liquid suspensions or aerosols containing these materials more toxic than their molecular or ionic forms. It necessitates a development of analytical techniques for highly sensitive detection and determination of nanoparticles. Different methods were suggested for this purpose [1]. One of them is based on Surface Plasmon Microscopy (SPM) [2–8]. SPM [9] is based on the transduction of changes of deviation from the surface plasmon resonance conditions into the changes of the reflected light intensity which is captured by a two-dimensional image sensor.

In the typical SPM arrangement, incident light is coupled to the plasmonic sensor layer through a glass prism. Under the conditions of surface plasmon resonance (SPR), where the wave vector of impinging light corresponds to the wave vector of surface plasmons, the energy of the incident light is coupled to the surface plasmon wave which is propagating along the interface and decays exponentially to both sides of it creating an evanescent field. The plasmon propagation and resonance conditions are influenced mainly by the dielectric permittivity of dielectric medium, which is contacting metallic layer, but only within the volume of penetration of evanescent field. Since the penetration depth value is a fraction of the wavelength of incident light, SPM provides

✉ Vladimir M. Mirsky  
mirsky@b-tu.de

<sup>1</sup> MIVITEC GmbH, Wamslerstr. 4, 81829 Munich, Germany

<sup>2</sup> Department of Biotechnology, Brandenburg University of Technology Cottbus – Senftenberg, Grossenhainerstr. 57, 01968 Senftenberg, Germany

<sup>3</sup> Leibniz Institute for Analytical Sciences (ISAS), Bunsen-Kirchhoff-Str. 11, 44139 Dortmund, Germany

<sup>4</sup> Institute of Hydrochemistry, Technical University of Munich, Marchioninstr. 17, 81377 Munich, Germany

an exceptional sensitivity for the nanoscale changes on this metal/dielectric interface. Due to these properties SPM is widely used in surface science and in bioanalytical chemistry, particularly in chemo- and bio-sensors [10, 11].

Because the matching of the wave vectors is only possible in conditions of total internal reflection, which implies large incidence and reflection angle of the light beam, the resonance occurs only in the small angular range. This leads to the low numerical aperture of this optical system and to the correspondingly low optical resolution of SPM in comparison with classical optical microscope. Due to this reason SPM is applied mainly for characterization of homogenous films when a high resolution is not required [11] and is frequently called as SPR-imaging instead of SPM or SPR-microscopy. On the other hand, the low lateral optical resolution, which is complicated by plasmon propagation, can be outweighed by extremely high sensitivity in transversal direction. A complex interaction of propagating surface plasmons with nanoscale objects on the sensor interface leads to intensive scattering which can be detected by image sensor. This effect allows one to use SPM for detection of single nanoparticles adsorbed on the sensor surface.

Two approaches for the application of SPM for detection of single nanoparticles were reported. While both are based on the excitation of surface plasmons in Kretschmann configuration, the optical system used for coupling and imaging of sensor surface under conditions of plasmon resonance can be either implemented by using separate objectives and camera tilted according to Scheimpflug principle (Fig. 1, left) [2, 3] or by using the high-numerical aperture (high-NA) microscopy objective which is applied simultaneously for the excitation and imaging (Fig. 1, right) [12, 13]. The latter approach allows one to reach a co-planarity of all optical planes thus leading to highly resolved low distortion images. However, this leads to the severe limitation of the field of view which is in this case typically smaller than  $100 \times 80 \mu\text{m}$  ( $< 0.01 \text{ mm}^2$ ). Using high-NA objective approach, a detection of single organic and metallic nanoparticles [4], viruses and DNA molecules [5, 6] as well as of electrochemical reactions catalyzed by single nanoparticles [7, 8] were demonstrated.

The classical SPM (Fig. 1, left) has essentially lower magnification and resolution of optical system but correspondingly much larger field of view: typical SPR-imaging setups monitor SPR signals from the surface of over  $20 \times 20 \text{ mm}$  ( $400 \text{ mm}^2$ ) which is four orders of magnitude larger than that of the high-NA based SPM setups. The relative light intensity changes due to adsorption of single nanoparticles are small and only a few times higher than the background noise [2, 3]. However, despite the lower resolution and signal to noise ratio (SNR), classical SPM has the advantage of the larger field of view. This leads to the lower detection limit in analysis of diluted suspensions of nanoparticles, to the higher dynamic range of counting of single nanoparticles which increase

essentially the concentration range of analyzed suspensions and to the possibility to make quantitative statistical analysis. In the current work the optical setup with a compromised value of the field of view of about  $1.0 \times 1.5 \text{ mm}$  was used. This is more than hundred times larger than that in the high-NA based SPM setups. Correspondingly hundreds times more nanoparticles—over tens of thousands of adsorbed nanoparticles—can be detected in one measurement, still maintaining a single nanoparticle resolution. Such a boost of dynamic range makes the manual data analysis impractical and necessitates the development and application of highly efficient algorithms for automated image analysis [3, 14].

In this work we present a computer assisted method for detection and characterization of single nanoparticles, adsorbing on the sensor surface. The method was validated on computer generated images and by comparison with manual image analysis. Then it was applied for analysis of SPM data on adsorption of gold and silver nanoparticles from aqueous suspensions as well as soot and NaCl nanoparticles from air. The suggested computer assisted detection and quantification of NPs in combination with the large detection area of SPM in classical arrangement allows one a high-throughput and accurate assessment of very different NPs samples in the wide concentration range.

## Experimental

The slope of the SPR curve and, correspondingly, the absolute value of SPR reflected light intensity signal is maximal at approximately 0.3–0.5 of SPR reflectivity [11]. However, taking into account the relative changes (the ratio of signal changes to the mean signal value), SPR conditions much closer to the SPR minima are preferred [15]. Moreover, in close vicinity to SPR conditions, the intensity of the reflected light tends towards zero thus decreasing the background level at which the small changes, caused by nanoparticles adsorption, are registered. Because of sharp dependence of the SPR dip on the wavelength and angle of the incident light, an application of a low divergence monochromatic light is required. The measurements were performed at the angle of SPR minima or at  $0.1$ – $0.3^\circ$  smaller angle.

A description of the principal set-up is given elsewhere [2]. For the current application in liquid samples the redesigned and optimized setup, developed within NANODETECTOR-project ([www.nanodetector.eu](http://www.nanodetector.eu)), was used. In this case the 642 nm SM-fiber coupled laser diode (LP642-SF20 from Thorlabs, [www.thorlabs.com](http://www.thorlabs.com)) was used as a light source. The collimated and polarized light beam is directed onto the plasmonic sensors consisting of SF-10 glass prism ( $n=1.72$ ) coated by 45–50 nm gold layer with 3 nm Ti adhesive layer (provided by Phasis, [www.phasis.ch](http://www.phasis.ch)). Image sensor chip “Aptina MT9P031112STM” with resolution of  $2592 \times 1944$

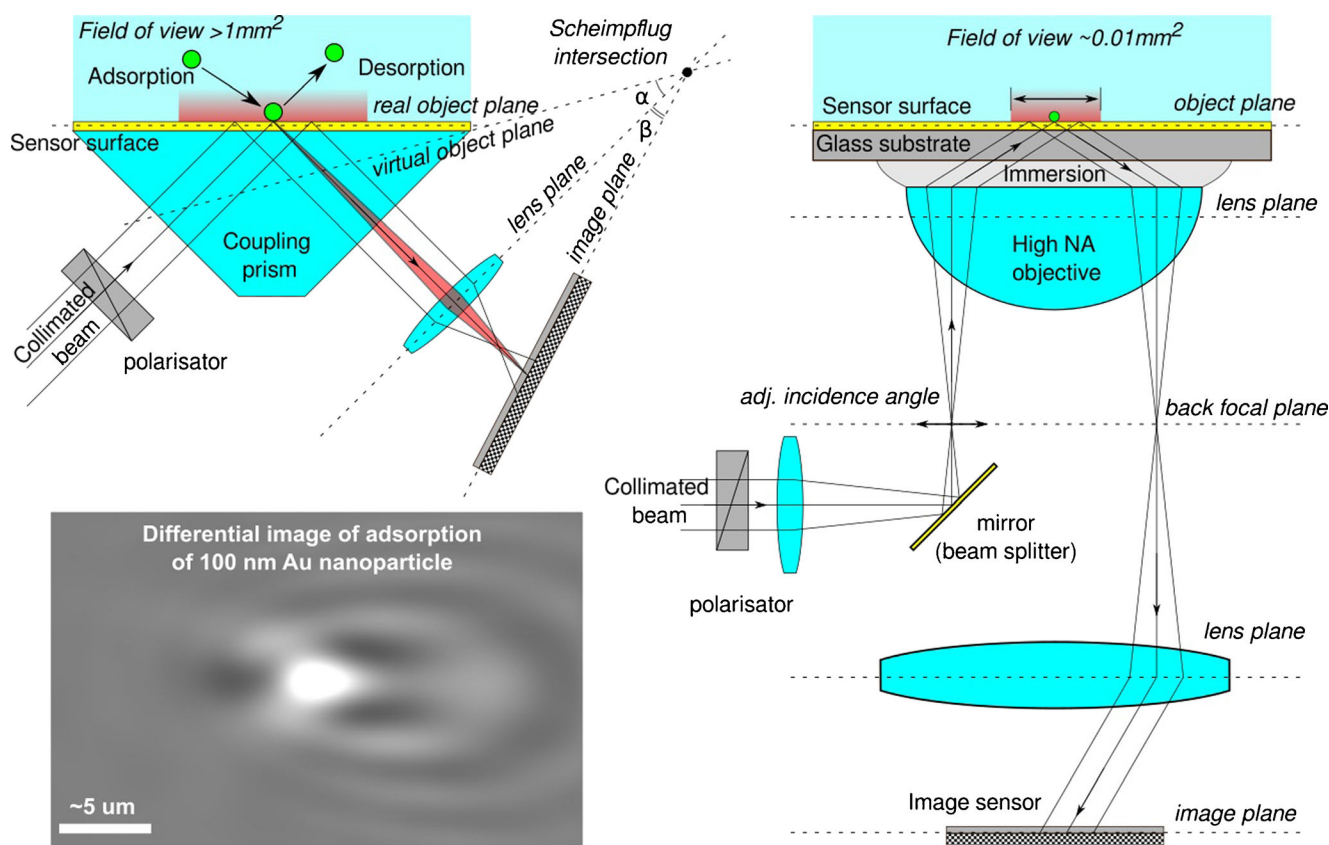


**Fig. 1** Two arrangements for surface plasmon microscopy. Inset: averaged differential SPM image of gold nanoparticle

and pixel size of  $2.2 \mu\text{m}$  was used ([www.aptina.com](http://www.aptina.com)). The images were collected at the frequency of 15 frames per second by Beagleboard-XM single-board computer ([www.beagleboard.org](http://www.beagleboard.org)) and averaged over 16 consecutive frames. Then the averaged frame was transferred to PC and saved for further analysis.

Before measurements the gold surface was cleaned using freshly prepared “piranha solution” (1:3 (v:v) mixture of  $\text{H}_2\text{O}_2/\text{H}_2\text{SO}_4$ ). *Caution: Piranha solution reacts violently with most organic materials and must be handled with extreme care.* Then the sensors were rinsed thoroughly with water and dried at room temperature. For the better adsorption of negatively charged nanoparticles the gold surface was functionalized by deposition of self-assembled monolayer of amino-modified 16-amino-1-hexadecanethiol (Prochimia, [www.prochimia.com](http://www.prochimia.com)) from 1 mM solution in ethanol during 12 h. Citrate stabilized silver and gold nanoparticles of different sizes were purchased from Sigma-Aldrich ([www.sigmaaldrich.com](http://www.sigmaaldrich.com)). The optical setup was installed so that the gold coated sensor faces upwards. The measurements in liquid were performed in a droplet of buffer solution containing 1.2 mM phosphate and 0–50 mM NaCl, pH 7.4. After adjustment of the SPR angle associated with the used buffer, nanoparticles suspended in the same buffer were injected carefully into the droplet to reach the final

concentration in the range of  $10^7$ – $10^9$  particles/mL in the droplet. During the adsorption of nanoparticles the sequence of images from SPM was captured and saved. The stock concentrations of nanoparticles were taken from supplier data. Before measurements,  $\xi$ -potentials of nanoparticles and size distributions were controlled using Zetasizer Nano ZS (Malvern Instruments, [www.malvern.com](http://www.malvern.com)) and found to be in agreement with values provided by supplier.

For aerosol measurements, the SF-10 prism was replaced by BK-7 glass prism. The surface was imaged by a macroobjective Canon EF 50/2.5” (Canon, [www.canon.com](http://www.canon.com)) with the magnification factor  $\sim 2$  onto a CMOS-Camera. Laser diode HL6750 ( $\lambda=685 \text{ nm}$ , Oclaro/Optnext [www.oclaro.com](http://www.oclaro.com)) was used as the light source. The driving current was modulated at a frequency of about 500 MHz in order to remove speckles. The gold layer was deposited on a 1 mm thick slide of SF-10 using 5 nm Ti adhesive sublayer (see above). The slide was contacted with prism using RI matching immersion oil (Cargille, [www.cargille.com](http://www.cargille.com)). The aerosol nanoparticles were charged and moved to the sensor surface by electric field applied between gold layer and an electrode placed at the distance of  $\sim 10 \text{ mm}$  parallel to the sensor surface. Modified LaMer-Sinclair generator [16] was used for generation of airborne sodium chloride particles. Soot particles were produced applying a spark discharge generator

(Gfg 1000, Palas, [www.palas.de](http://www.palas.de)). Size selection and quantification of aerosol particles was performed using differential mobility analyzer (type 3071) and condensation particle counter (type 3775, both TSI, [www.tsi.com](http://www.tsi.com)).

For the validation and benchmarking purposes, the separate software for manual processing and counting of nanoparticles as well as for generation of simulated image sequences was developed. The software for manual counting provides a registration of coordinates of each visually detected nanoparticle. The computer generated images were formed by random distribution of averaged patterns of nanoparticles (e.g., Fig. 1, inset) with defined signal to noise ratio over the noisy background image.

## Data analysis

**Image enhancement** Detection of nanoparticles in SPM records is based on analysis of collective temporal and spatial intensity variations [2]. However, the amplitude of the intensity step for small particles exceeds the background noise level only slightly; therefore the patterns from adsorbed nanoparticles are not visible in the raw SPM images [14]. The main goal of the image enhancement is an improvement of signal to noise ratio. In order to decrease the camera noise and to minimize variations caused by fluctuations and drifts of the image of the sensor surface, pixel by pixel averaging over several frames and referencing of the averaged image to preceding averaged image was performed. The resulting sequence of differential averaged images displays only changes between subsequent averaged frames. The performed suppression of static and slightly drifted background makes possible a visualization of adsorption of nanoparticles as an appearance of bright or dark spots (Fig. 2 left) which are sometimes surrounded by rings [2, 3, 14].

The next step includes a digital filtration based on characteristic features of patterns of nanoparticles. There are several specific features of particle detection on SPR images. The signals of bond particles are strongly localized in time and space while the intensity value of the central blob can be close to the noise level of background, and the magnitude of the variation of the ring pattern has the same scale as that for the background pattern (Fig. 2, left).

A number of spatial filters [17, 18] for enhancement of SPR images were evaluated: mean, Gaussian, DoG (difference of Gaussians), median and fast Fourier transform (FFT)-based frequency methods. The main criterion for the selection of the enhancement method was an increase of the signal to noise ratio (SNR). Global FFT methods amplified not only the particle pattern but also structural noise. The best results were obtained by local averaging methods (Fig. 2 right). Such a mean filter is a scale dependent local averaging operation where the value of each pixel is replaced by the average value

through all values of the local neighborhood. Gaussian filter can be regarded as weighted averaging with the weights chosen according to the shape of the Gaussian function: the original pixel in center receives the highest weight and with an increase of the distance from the central pixel the weight decreases. Both averaging filters can be implemented as the convolution of the image  $I(x,y)$

$$I(x,y)*m(x,y) = \sum_{i=-w/2}^{w/2} \sum_{j=-w/2}^{w/2} I(x+i,y+j)m(i,j)$$

with normalized mask of size  $w$  calculated as  $m(x,y)=1/w^2$  for mean filter and

$$m(x,y) = G(x,y) = \frac{1}{2\pi\sigma^2} e^{-\frac{x^2+y^2}{2\sigma^2}}$$

for Gaussian filter [17, 18]. They work as low pass filters, i.e., remove higher frequency components, blur sharp elements and edges. They reduce contrast but allow the low-frequency features to “pass” through the filter unchanged. Local space filters are very sensitive to the choice of scale: an application of the mask with a wrong scale may vanish particle signals with the background. In order to let all particles patterns to pass through the average filters, the size of convolution mask should not exceed the radius of the smallest particle pattern in the SPM record. In the current work Gaussian and mean filters were used with kernel size of the order of optical resolution of SPM.

**Particles detection** Typical pattern of adsorbed nanoparticle can be represented as a central blob (bright or dark) surrounded by one or more rings [2, 3, 14]. Such patterns vary for different imaging conditions and different nanoparticles. Depending on the signal intensity and background noise ratio, the rings and the brightness of the blob can be severely suppressed. While some images of nanoparticles look like just as large white or black blobs of different intensity and diameter without surrounding ring pattern, others display only a part of the rings etc. To detect all kinds of these images several numerical methods were evaluated and combined.

The detection of nanoparticles starts by selection of pixels which can be a part of the image of adsorbed nanoparticle, this is performed using threshold of intensity histogram of differential images. However, an intensity increase can be caused not only by binding particle but also by an increase of the local noise or by an appearance of some unrelated disturbances. Therefore, all candidate pixels should be checked for the presence of blob or rings. Statistical analysis of pixels intensity in several consecutive frames allows us to exclude a random temporal intensity increase. To satisfy sufficient spatial extent of the detected spot with intensity

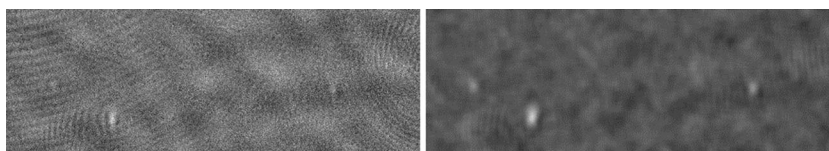


**Fig. 2** Grouped, normalized and standardized differential images with one intensive and two weak footprints from adsorbed nanoparticles before (*left*) and after (*right*) enhancement by Gaussian filter

increase, the pixel-by-pixel analysis of intensity was followed by the nearest neighbor classification using seed-growing algorithm. The obtained spots which have smaller or larger size than the predefined patterns of nanoparticles can be neglected. If the group of connected pixels satisfies particle size criterion, the local signal to noise ratio ( $SNR_{max}$ ) is checked to satisfy an intensity step criterion: if  $SNR_{max}$  overcomes statistical standard deviation of the background noise, the intensity change in this group is considered as the signal caused by adsorption of nanoparticle.

**Intensity threshold** An identification of prominent pixels which may be a part of the image of adsorbed nanoparticles, reduces significantly the amount of positions for further analysis and classification with numerically expensive methods. In order to avoid an exhaustive numerical analysis and to decrease a number of false detections, the prominent pixels are identified beforehand by maximum intensity threshold. The threshold value  $I_{th}$  for numerical calculations is determined by the input parameter  $k$ , standard deviation  $stdev$  and average value of the pixel intensity  $I_{mean}$  as:  $I_{th} = I_{mean} + k * stdev$ . The pixels where  $I > I_{th}$  have intensity changes at least  $k$ -times stronger than the standard deviation caused by pixel noise. Such pixels constitute a set of pixels selected for the further analysis and form a binary image, which strongly depends on the quality of the input greyscale images and determines the computational speed and accuracy of detection. A nanoparticle missed at this step cannot be recovered later on. Therefore this step is crucial to all further processing and a low value of the intensity threshold ( $k \leq 4$ ) was chosen. It elevates the number of false positive events which will be filtered out during the further analysis steps.

**Blob recognition** The spatial criteria for detection of nanoparticle images in differential SPM image is change of brightness of a small group of neighboring pixels, which form a blob with a spatial extent with some radius  $r$ . Usually objects display not a sharp drop-off edges but rather a gradual transition between different intensity levels. To describe the variation of the gradient caused by a random noise one can consider differentiated Gaussian. A differentiation of the gradient gives the second derivative, i.e., Laplacian of Gaussian. The white (black) blob can be detected by convolution of the input

image  $I(x,y)$  with negative (positive) normalized Laplacian of Gaussian (LoG),

$$\psi_{\sigma} = -\sigma^2 \nabla^2 G = \frac{1}{\pi \sigma^2} \left[ 1 - \frac{x^2 + y^2}{2\sigma^2} \right] e^{-\frac{x^2 + y^2}{2\sigma^2}}$$

which is known as Marr-Hildreth Operator (due to shape of this function it is also called as Mexican Hat Wavelet) [19]. Defining the scales of interest we do not need to perform the total transformation but only convolve the image using the kernel functions with corresponding scale.

**Ring pattern recognition** To find weaker patterns (e.g., without pronounced central blob), an image analysis based on the Scaling Index Method (SIM [20]) was applied. The SIM allows us to distinguish points, lines and unstructured background. A 2D image is described in the SIM as a set of points in virtual 3D space with two spatial coordinates  $(x, y)$  and a value of the intensity of each pixel  $I(x, y)$  as a third dimension. Thus, both space and intensity information can be combined in the three-dimensional vector  $\vec{p}_i = (x, y, \nu(x, y))$  while the image can now be regarded as a set of  $N$  points  $P = \{\vec{p}_i\}$ ,  $i = 1, \dots, N_{pixels}$ . For each pixel  $p_i$  the logarithmic gradient  $\alpha_i$ , called scaling indices, is calculated as:

$$\alpha_i = \frac{\partial \log \rho(\vec{p}_i, r)}{\partial \log r}, \quad \rho(\vec{p}_i, r) = \rho(\vec{p}_i, r) = \sum_{j=1}^{N_{pixel}} e^{-\left(\frac{d_{ij}}{r}\right)^2}.$$

Here  $d_{ij} = \|\vec{p}_i - \vec{p}_j\|_2$  is the Euclidean distance between two points in the virtual 3D space, and  $r$  is the radius of interest which is equal to the thickness of the ring line in particle pattern. Due to its Gaussian shape the weighted cumulative point distribution  $\rho$  causes SIM to be a local method: the value of the scaling index depends on the number of the neighbors only in a small vicinity of the point for which the gradient  $\alpha$  is calculated. The SIM gives an alternative representation of the images: the value of  $\alpha \approx 0$  corresponds to unstructured background, while  $\alpha \approx 1$  corresponds to line structure (ring pattern in our case) and  $\alpha \approx 2$  corresponds to 2D spot.

**Intensity step** The basic evidence for nanoparticle adsorption is an intensity step within few consecutive frames [2]. Student's Two Mean  $t$ -Test was applied to the time-averaged intensity of several predecessor and successor frames of the currently observed image to detect statistically significant

increase of pixels intensity.  $t$ -statistic for the most general case of unequal sample size and unequal variances (Welch's  $t$ -test [21]) was calculated:

$$t = (\bar{X}_a - \bar{X}_b) / \sqrt{\frac{s_a^2}{N_a} + \frac{s_b^2}{N_b}}$$

Here  $\bar{X}_i, s_i^2, N_i$  are the mean value, the variance and the size of the intensity value before ( $i = b$ ) and after ( $i = a$ ) the intensity step. Giving the value of the intensity step and the significance level, one can use this approach as a time-domain binary filter to find pixels probably belonging to the images of adsorbed nanoparticles.

**Seed growing algorithm** To group pixels with increased intensity the seed growing algorithm [22] was applied. The pixels selected as probably belonging to the nanoparticle images in the previous steps, were used as seeds for the region growing process. According to the region membership criterion, connected pixel groups grow from these seed points. In this work 4-connected neighborhood (each pixel with coordinates  $(x \pm 1, y)$  or  $(x, y \pm 1)$  is connected to the pixel at  $(x, y)$ ) was applied. By examining pixels in 4-connected neighborhood of seed points pixels are merged into groups.

### Validation of the numerical detection of nanoparticles

The validation of the presented numerical procedure for particle detection was performed by two ways: i) a comparison with computer generated images consisting of background and random spatial/temporal distribution of images of bound nanoparticles; ii) a comparison with a manual assessment of actual experimental images. The coincidence of the detected nanoparticles was counted as a true-positive event, the non-intersected numerically detected nanoparticle was considered as a false-positive and the non-intersected manually detected nanoparticle was considered as a false-negative.

**Validation by comparison with simulated images** was performed using two sequences consisting of 200 images. The background with the size of the actual SPM images was filled with a white random noise. For the temporal distribution the Poisson distribution around the mean value of ten nanoparticles per frame and signal to noise ratio of 3.0 and 1.0 (Fig. 3 first row) was used. The determined amount of real nanoparticle images (extracted from the experimental images and averaged) was randomly distributed over the background image. In Fig. 3 the number of the detected nanoparticles in the current frame ( $N_p$ , second row) and the cumulative number of the detected nanoparticles up to the current frame ( $N_{p\_cum}$ , third row) are shown. In both cases the number of the detected

nanoparticles per frame oscillates around the defined average value  $N_p = 10 \pm 7$  (Fig. 3 second row). The calculated cumulative number of nanoparticles per 200 frames is  $N_{p\_cum} \approx 2000$ , which is approximately equal to the product of the given average number of nanoparticles per frame multiplied to the number of frames (200), with 6 % underestimation for  $SNR = 3$  and 5 % overestimation for  $SNR = 1$  (Fig. 3, third row).

Validation with simulated differential SPM images demonstrated two main sources for the false positive detections which limit the accuracy of numerical detection. The underestimation of the nanoparticles quantity in the case of  $SNR = 3$  is mainly due to nanoparticles which bind very close to each other. In this case their images coalesce and a single nanoparticle is detected. In the case of high background noise ( $SNR = 1$ ) the ring pattern, usually much weaker than the central blob, are suppressed to the noise level so that the nanoparticles are detected only by their central blobs. At the same time, the background noise at low  $SNR$  can also form bright spots, thus leading to false-positives and overestimation of total amount of adsorbed nanoparticles.

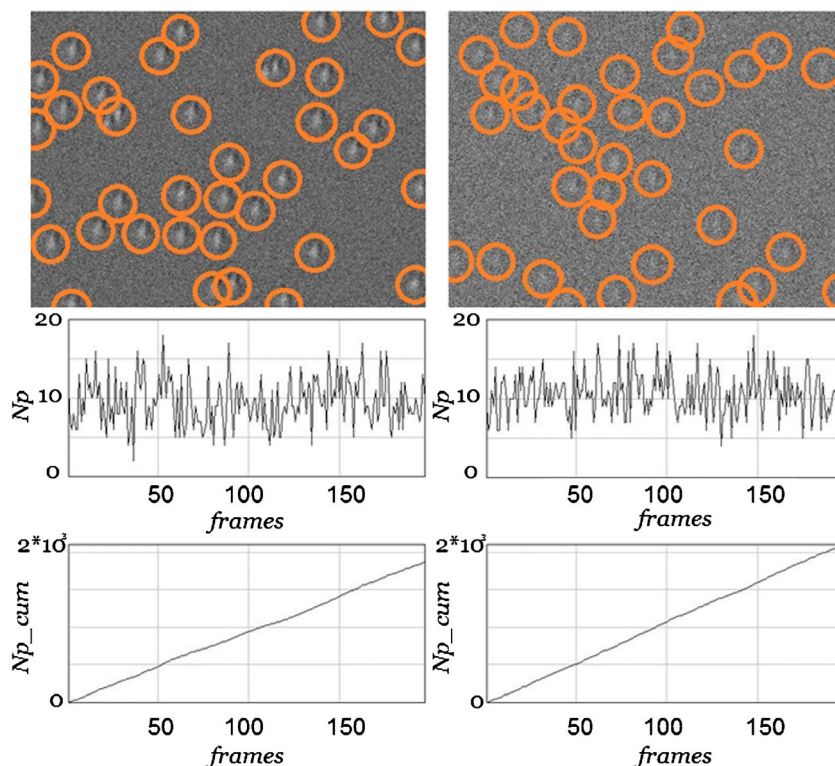
**Validation by comparison with manual detection** in real experiments was performed for three series containing 500–1000 frames each, with different number of adsorbed nanoparticles per frame. Some of these image sequences contain large regions with structured background noise. The number of nanoparticles in the current frame ( $N_p$ ) and the cumulative number of all nanoparticles ( $N_{p\_cum}$ ) for one of experiments is shown in the Fig. 4: the left panels were obtained by manual detection of nanoparticles while the right panels present the results of numerical detection. In both cases the average value of  $N_p$  oscillates around the same average value, and the obtained dependencies of  $N_{p\_cum}$  for manual and numerical detections are very close: the difference between the quantities of manually and numerically detected nanoparticles in all experimental images was below 9 %.

It is to note that in current work the focus is on the image analysis aspect. The phenomenology of the experimentally observed behavior of nanoparticles sorption is quite complex: some nanoparticles slide across the surface or oscillate near it. Such nanoparticles may be detected several times giving a small additional source of false positive events.

### Application examples

Theoretical analysis of SPM images of adsorbed nanoparticle predicts that the image shape and intensity are dependent on the material and size of the nanoparticle [23]. However, because of the finite resolution and inevitable aberrations of optical system and substantial level of the background noise, an analysis of the exact image shape can be hardly done. Principal Component Analysis did not find any hidden

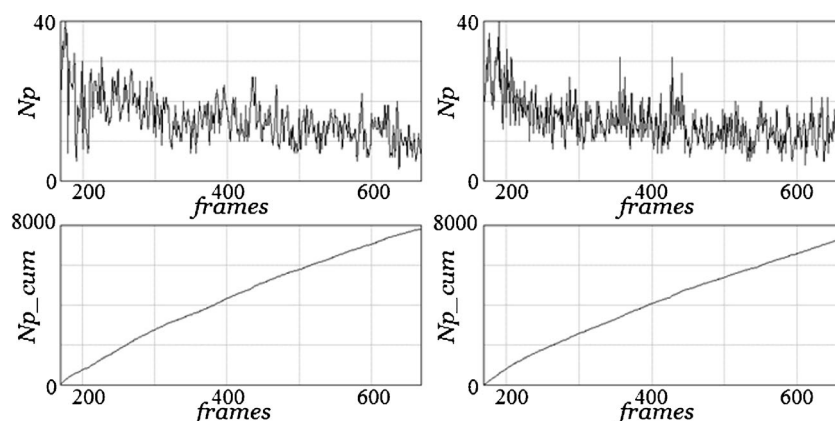
**Fig. 3** Validation of nanoparticle detection using computer generated images. Detected nanoparticles are indicated by circles (upper row,  $SNR=3$  (left) and  $SNR=1$  (right)). The number of numerically detected nanoparticles in the current frames  $N_p$  (middle row). The bottom row indicates the cumulative number of the detected nanoparticles up to the current frame  $N_{p\_cum}$



features within introduced image descriptors and showed the best clustering in the feature space of maximal signal to noise ratio ( $SNR_{max}$ ) for the detected images of NPs. This value represents the ratio of intensity step, which is caused by nanoparticle adsorption, to the local level of background noise. Thus the image intensity was proved to be the best descriptor.

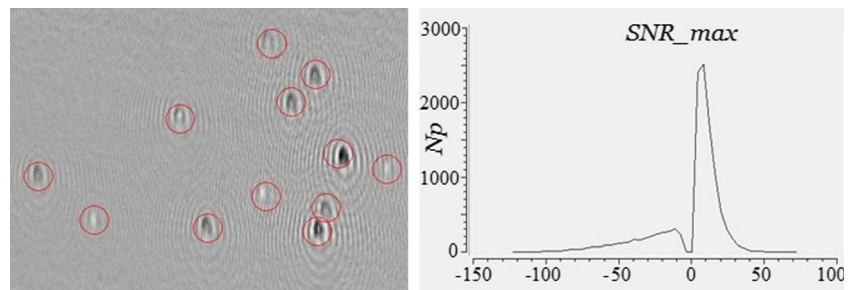
Experimental images obtained for gold NPs, adsorbing from the mixture of 40 to 100 nm, is shown in Fig. 5 (left). According to previous experimental data [2, 3] and theoretical analysis [23], the smaller is the particle, the weaker and smaller is its image in differential SPM image. In Fig. 5 the 40 nm nanoparticles produce weak signals which look like small white spots without ring patterns. The 100 nm nanoparticles provide strong signals in the form of large black central blob surrounded by ring pattern.

**Fig. 4** Comparison of manual (left) and numerical (right) detection of images of nanoparticles in experimental SPM records in the frames (upper panels) and cumulative values for the whole SPM record (lower panels)



More detailed analysis can be performed using histograms of intensity. Figure 5, right, demonstrates the results of automated analysis of SPM records for these types of gold NPs: two obvious peaks of  $SNR_{max}$  corresponding to these types of NPs are clearly seen. The same approach was applied also for aerosols (Fig. 6). The large difference in the refractive index of salt and air as well as soot and air leads to high signals from adsorbed nanoparticles. For airborne NaCl—NPs the image intensity depends linearly on the size of nanoparticles (Fig. 6 left, middle). The soot particle counting rate depends linearly on the number concentration of the nanoparticles in the aerosol (Fig. 6, right). Application of the threshold to the histogram allows the suppression of the weak false positive signals caused by background fluctuations. The linear dependence of adsorption rate of nanoparticles on their number concentration

**Fig. 5** Example of the experimental image obtained for the mixture of 40- and 100 nm gold nanoparticles (*left*, images of nanoparticles are indicated by circles) and a histogram of maximum of signal to noise ratio  $SNR_{max}$  for the detected images (*right*)



provides a possibility to use this approach for quantitative measurements of number concentrations of nanoparticles.

The adsorption rate of NPs from aqueous suspensions is defined by their free diffusion due to Brownian motion and was in the range 0.1–10 NPs per s per  $\text{mm}^2$  for number concentration in range  $10^6$ – $10^8$  particles/mL. To avoid diffusion limitations, soot and NaCl nanoparticles in air were ionized and attracted to the surface by the external electrical field. Correspondingly, the counting rate reached to 5 NPs per s per  $\text{mm}^2$  already at the number concentration of  $10^3$  particles/mL (see Fig. 6).

The presented method of analysis was also applied for many other types of nanoparticles, for example for silver and polystyrene NPs of different size. The lowest size of nanoparticles which can be detected using the presented computer assisted analysis depends on the difference in dielectric permittivity of the material of nanoparticle and environment and is about 30 nm for plasmonic nanoparticles and 60 nm for polystyrene nanoparticles.

## Conclusions

We describe computer assisted numerical method for automated detection and quantification of NPs imaged by differential SPM during adsorption from aqueous suspensions and aerosols. The method consists of frame-by-frame image processing, which includes an image enhancement, a global statistical analysis of images followed by detection and a local analysis

of images of individual nanoparticles. Different image enhancement methods were evaluated; the local mean- and Gaussian filters were found to be the most useful for detection of nanoparticles. The detection is based on the fast temporal and spatial intensity change and specific spatial pattern in differential SPM images caused by adsorption of nanoparticle. However, not all nanoparticles have identical image patterns. The central blob or surrounding ring structure can be suppressed or distorted by background noise and experimental artifacts. The suggested combination of different image analysis approaches provides a reliable detection of even weak or distorted images of NPs. For the characterization of images of detected nanoparticles different statistical characteristics were evaluated;  $SNR_{max}$  was found to be the most informative. Clustering of its value for detected nanoparticles allows one to distinguish NPs from false detected background artifacts.

The numerical method was validated by an independent manual analysis of experimental data and by using computer generated image sequences with a randomized amount and positions of NPs. Depending on the type and size of NPs and on the level of the background noise, a probability of recognition of up to 90–95 % can be reached. The use of classical SPM configuration with a large sensor area allows one a surface patterning [24–26] for preparation of SPR-sensor arrays. Different functionalization of sensing elements opens the way for analysis of materials of nanoparticles. Also in this case can be used the suggested method for detection and identification of NPs.

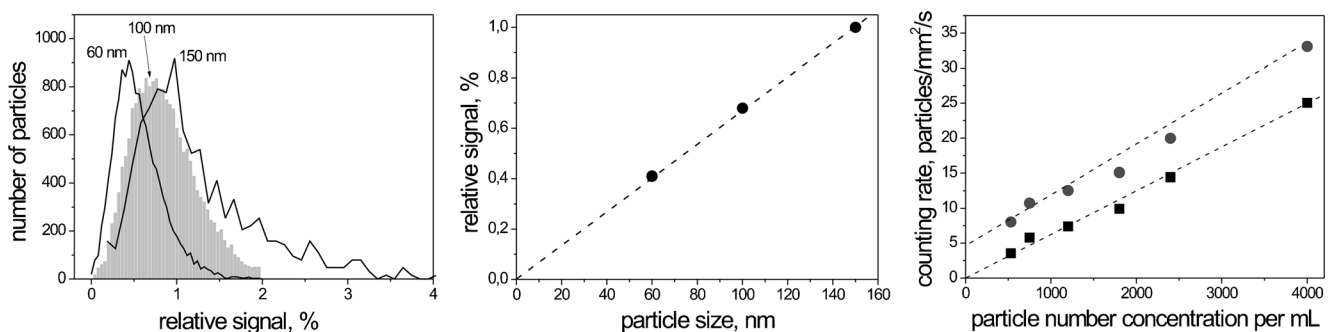


**Fig. 6** The histogram of SPR signals due to adsorption of NaCl nanoparticles from aerosol (*left*), the dependence of the mean signal value on the size of these nanoparticles (*middle*) and the concentration

dependence of the adsorption rate on the aerosol number concentration (*right*) before (*circles*) and after (*squares*) correction of background



**Acknowledgments** The work was supported by FP7 EC Project “Nanodetector” (FP7-NMP-2011-SME-5, #280478). The authors are grateful to the partners of the Project “Nanodetector” for fruitful collaboration during the development and assembly of the experimental device. We acknowledge K. Tonder, F. Klemm, V. Scherbahn and M. Michling for assistance in the experimental measurements and manual verification of the numerical particle detection as well as an assistance of students of BTU Cottbus—Senftenberg in the manual validation of the counting software.

## References

- Hasselov M, Readman JW, Ranville JF, Tiede K (2008) Nanoparticles analysis and characterization methodologies in environmental risk assessment of engineered nanoparticles. *Ecotoxicology* 17:344–361
- Zybin A, Kuritsyn YA, Gurevich EL, Temchura VV, Überla K, Niemax K (2010) Real-time detection of single immobilized nanoparticles by surface plasmon resonance imaging. *Plasmonics* 5:31. doi:10.1007/s11468-009-9111-5
- Gurevich EL, Temchura VV, Überla K, Zybin A (2011) Analytical features of particle counting sensor based on plasmon assisted microscopy of nano objects. *Sensors Actuators B Chem* 160:1210–1215. doi:10.1016/j.snb.2011.09.050
- Halpern AR, Wood JB, Wang Y, Corn RM (2014) Single-nanoparticle near-infrared surface plasmon resonance microscopy for real-time measurements of DNA hybridization adsorption. *ACS Nano* 8(1):1022–1030. doi:10.1021/nn405868e
- Yu H, Shan X, Wang S, Chen H, Tao N (2014) Plasmonic imaging and detection of single DNA molecules. *ACS Nano* 8(4):3427–3433. doi:10.1021/nn4062885
- Wang S, Shang X, Patel U, Huang X, Lu J, Li J, Tao N (2010) Label-free imaging, detection, and mass measurement of single viruses by surface plasmon resonance. *PNAS* 107(37):16028–16032. doi:10.1073/pnas.1005264107
- Fang Y, Wang W, Wo X, Luo Y, Yin S, Wang Y, Shan X, Tao N (2014) Plasmonic imaging of electrochemical oxidation of single nanoparticles. *J Am Chem Soc* 136:12564–12587. doi:10.1021/ja507097y
- Shan X, Diez-Pérez I, Wang L, Wiktor P, Gu Y, Zhang L, Wang W, Lu J, Wang S, Gong Q, Li J, Tao N (2012) Imaging the electrocatalytic activity of single nanoparticles. *Nat Nanotechnol* 7:668–672. doi:10.1038/nnano.2012.134
- Rothenhauesler B, Knoll W (1988) Surface plasmon microscopy. *Nature* 332:615–617. doi:10.1038/332615a0
- Homola J (2008) Surface plasmon resonance sensors for detection of chemical and biological species. *Chem Rev* 108:462–493. doi:10.1021/cr068107d
- Brockman JM, Nelson BP, Corn RM (2000) Surface plasmon resonance imaging measurements of ultrathin organic films. *Annu Rev Phys Chem* 51:41–63. doi:10.1146/annurev.physchem.51.1.41
- Somekh MG, Liu S, Velinov TS, See CW (2000) High-resolution scanning surface-plasmon microscopy. *Appl Opt* 39:6279–6287. doi:10.1364/AO.39.006279
- Huang B, Yu F, Zare RN (2007) Surface plasmon resonance imaging using a high numerical aperture microscope objective. *Anal Chem* 79:2979–2983. doi:10.1021/ac062284x
- Weichert F, Gaspar M, Timm C, Zybin A, Gurevich EL, Engel M, Müller H, Marwedel P (2010) Signal analysis and classification for surface plasmon assisted microscopy of nanoobjects. *Sensors Actuators B Chem* 151:281–290. doi:10.1016/j.snb.2010.08.005
- Zybin A, Boecker D, Mirsky VM, Niemax K (2007) Enhancement of the detection power of surface plasmon resonance measurements by optimization of the reflection angle. *Anal Chem* 79:4233–4236. doi:10.1021/ac070074u
- Scheibel HG, Postendörfer J (1983) Generation of monodisperse Ag- and NaCl-aerosols with particle diameters between 2 and 300 nm. *J Aerosol Sci* 14:113–126
- Jain R, Kasturi R, Schunck BG (1995) *Machine vision*. McGraw-Hill. ISBN 0-07-032018-7
- Young IT, van Vliet LJ (1995) Recursive implementation of the Gaussian filter. *Signal Proc* 44:139–151. doi:10.1016/0165-1684(95)00020-E
- Lindeberg T (1998) Feature detection with automatic scale selection. *Int J Comput Vis* 30:7–116. doi:10.1023/A:1008045108935
- Räth C, Morfill G (1997) Texture detection and texture discrimination with anisotropic scaling indices. *J Opt Soc Am A* 14(12):3208–3215. doi:10.1364/JOSAA.14.003208
- Welch BL (1947) The generalization of “Student’s” problem when several different population variances are involved. *Biometrika* 34: 28–35. doi:10.2307/2332510
- Mat-Isa NA, Mashor MY, Othman NH (2005) Seeded region growing features extraction algorithm. *IJSIM* 13:61–70
- Demetriadou A, Komyshev AA (2015) Principles of nanoparticle imaging using surface plasmons. *New J Phys* 17:013041. doi:10.1088/1367-2630/17/1/013041
- Boecker D, Zybin A, Niemax K, Grunwald C, Mirsky VM (2008) Noise reduction by multiple referencing in surface plasmon resonance imaging. *Rev Sci Instrum* 79:023110
- Nizamov S, Scherbahn V, Mirsky VM (2015) Self-referencing SPR-sensor based on integral measurements of light intensity reflected by arbitrarily distributed sensing and referencing spots. *Sensors Actuators B Chem* 207:740–747. doi:10.1016/j.snb.2014.10.022
- Love JC, Estroff LA, Kriebel JK, Nuzzo RG, Whitesides GM (2005) Self-assembled monolayers of thiolates on metals as a form of nanotechnology. *Chem Rev* 105:1103–1170. doi:10.1021/cr0300789